第 30 卷第 12 期 无 机 化 学 学 报 Vol.30 No.12
2014 年 12 月 CHINESE JOURNAL OF INORGANIC CHEMISTRY 2872-2878

# 马来二腈基二硫烯镍(Ⅱ)配合物展现了介电反常和弛豫

段海宝* 于姗姗 周 宏
(南京晓庄学院生物化工与环境工程学院,南京 211171)

**摘要**: 合成并用 X-射线单晶衍射表征了一个离子对化合物 1,7-bis(1-methylimidazolium)heptane bis(maleonitriodithiolato)nickelate (**1**)的结构。沿着晶体学 *c* 轴方向,化合物 **1** 中的阴、阳离子分别排列形成波浪形的链。变温介电性质研究表明,化合物 **1** 在 90 ℃ 左右展现了介电态转变。我们将此转变归于化合物 **1** 中平衡阳离子的有序到无序转变。在低频区,化合物 **1** 出现了明显的介电弛豫过程,这与阳离子偶极运动有关。此外,DSC 研究表明,在第二个升温过程中,化合物 **1** 在 66 ℃ 和 130 ℃ 左右出现两步冷结晶。此种冷结晶现象在小分子化合物中很罕见,这与化合物 **1** 的较大粘度以及测试过程中的较快降温速率有关。

**关键词**: 金属二硫烯配合物; 介电反常; 介电弛豫; 晶体结构
**中图分类号**: O614.81+3 **文献标识码**: A **文章编号**: 1001-4861(2014)12-2872-07
**DOI**:10.11862/CJIC.2014.388

# A Bis(maleonitriledithiolato)nickelate Ion-Pair Compound Exhibiting Dielectric Anomaly and Relaxation

DUAN Hai-Bao* YU Shan-Shan ZHOU Hong
(*School of Biochemical and Environmental Engineering, Nanjing Xiaozhuang University, Nanjing* 211171, *China*)

**Abstract:** An ion-pair compound, 1,7-bis(1-methylimidazolium)heptane bis(maleonitriodithiolato)nickelate (**1**), was synthesized and single crystal structurally characterized. The bis (maleonitriodithiolato)nickelate anions and dication formed the wave-shape anion chain along *c*-axis direction, respectively. **1** undergoes a tunable transition at about 90 ℃ between high and low dielectric states at variable temperature, which probably arises from the order-to-disorder transformation of alkyl chains. The dielectric relaxation process in low-frequency region, attributed to the orientation polarization of the molecules dipoles, was observed and discussed. Furthermore, **1** exhibits cold crystallization around 66 ℃ and 130 ℃ during the second heating scan, and originated from fast cooling rate and the large viscosity. Such study provides a possible strategy to explore switchable dielectric material. CCDC: 1015809.

**Key words:** Metal-bis-dithiolene complex; dielectric anomaly; dielectric relaxation; crystal structure

## 0 Introduction

Dielectric materials are fundamental components of modern electrical and electric device[1-3]. Some special solid dielectrics have been widely used in microelectronic and electrical engineering. For example, a low-$\kappa$ dielectric is generally used to separate the conducting parts (such as the wire interconnects and transistors) from one another in digital circuits, reduces parasitic capacitance, enables faster switching speeds, decreases cross-talk noise and lowers heat dissipation in a microelectronic device[4-6].

收稿日期:2014-08-20。收修改稿日期:2014-09-17。
国家自然科学基金(No.21201103,21301093)资助项目。
*通讯联系人。E-mail:duanhaibao4660@163.com

At present, a lot of progress has been achieved in designing solid state dielectrics[7-13]. However, it still remains a challenge to design the crystalline solids possessing tunable dielectric states. Such dielectric behavior between high and low dielectric states, have been playing a momentous role in photo-electronic fields [14-16]. One of the most promising strategies to assemble such functional material, usually, is to design and synthesize molecule compounds with order-disorder structural transformations which can generally induces dielectric phase transition. Recently, some dielectrics with tunable dielectric states can be found in metal-organic frameworks (MOFs) in which the rigid cavities are generally filled by the guest molecules, such as lattice solvents or counterions. The order-disorder transition of the polar guest molecule in the rigid cavities leaded to striking dielectric anomalies[17-19]. Furthermore, some molecular motion associated rotational can induce the variation of the dielectric states. Among such molecules, the motion phase has been well recognized in plastic crystalline states such as hexamethylethane, cyclohexane, adamantane, and fullerene ($C_{60}$), where the structural flexible and spherical molecules have a tendency to form the motion phase[20]. In our and other groups previous study, bis-1,2-dithiolene complexes of transition metals have been widely studied due to their novel properties and application in the areas of conducting and magnetic materials, dyes, non-linear optics, catalysis and others[21-23]. Recently, we further designed and assembled some phase transition compounds by introducing molecular motion in such system[24-25]. Encouraged by our previous study and above-mentioned findings, in this paper, we present a new compound [1,7-bis(1-methylimidazolium)heptane] [Ni(mnt)$_2$] (**1**), which exhibits novel dielectric anomaly and relaxation.

## 1 Experimental

### 1.1 Chemicals and reagents

All reagents and chemicals were purchased from commercial sources and used without further purification. The starting materials disodium maleonitriledithiolate ($Na_2$mnt) and 1,7-bis(1-methylimidazolium)heptane dibromide were synthesized following the published procedures[26-28].

### 1.2 Physical measurements

Elemental analyses for C, H and N were performed with an Elementar Vario EL III analytic instrument. Powder X-ray diffraction (PXRD) data were collected on a Bruker D8 diffractometer with Cu $K\alpha$ radiation ($\lambda$=0.154 18 nm). FT-IR spectra were recorded on an IF66V FT-IR (4 000~400 cm$^{-1}$) spectrophotometer with KBr pellets. Thermogravimetric (TG) experiments were performed with a TA2000/2960 thermogravimetric analyzer from 38 to 800 ℃ at a warming rate of 10 K·min$^{-1}$ under a nitrogen atmosphere, and the polycrystalline samples were placed in an aluminum crucible. Differential scanning calorimetry (DSC) was carried out on Pyris 1 power-compensation differential scanning calorimeter in the range −85 ~ 230 ℃ for **1** and the warming/cooling rate is 10 K·min$^{-1}$ during two thermal cycles. Temperature and frequency dependent dielectric constant, $\varepsilon'$, and dielectric loss, tan$\delta$, measurements were carried out employing Concept 80 system (Novocontrol, Germany); the powdered pellet, with a thickness of ca. 0.50 mm and 78.5 mm$^2$ in the area, was coated by gold films on the opposite surfaces and sandwiched by the copper electrodes and the ac frequencies span from 1 to $10^7$ Hz.

### 1.3 Preparations for 1

$Na_2$mnt (456 mg, 2.5 mmol) and $NiCl_2\cdot 6H_2O$ (297 mg, 1.25 mmol) were mixed under stirring in MeOH (30 mL) at room temperature. Subsequently, a solution of 1,7-bis(1-methylimidazolium)heptane dibromide (2.5 mmol) in MeOH (15 mL) was added to the mixture, and the red precipitate was immediately formed, and washed with MeOH. The crude product was recrystallized in DMF (20 mL) to give dark-red crystals. Elemental analysis: Calcd. for $C_{23}H_{26}N_8NiS_4$ (%): C, 45.93; H, 4.36; N, 18.63. Found(%): C, 45.72; H, 4.54; N, 18.39. IR spectrum (KBr disc, cm$^{-1}$): 3 113 m, 2 926m, 2 196s, 1 569m, 1 474s, 1 145m, 830m.

### 1.4 X-ray crystallography

Selected crystals of **1** were centered on a Bruker

SMART APEX CCD-based diffractometer with graphite-monochromatic Mo $K\alpha$ radiation ($\lambda$=0.071 073 nm). Measurements were performed at 296 K. The data collection routine, unit cell refinement, and data processing were carried out with the program CrysAlis[29]. Structures were solved by the direct method and refined by the full-matrix least-squares procedure on $F^2$ using SHELXL-97 program[30]. The non-Hydrogen atoms were anisotropically refined using the full-matrix least-squares method on $F^2$. All H atoms were placed at calculated positions and refined riding on the parent atoms. Details of the crystallographic parameters, data collection, and refinements for **1** are summarized in Table 1. Selected bond lengths and angles are listed in Table 2.

CCDC: 1015809.

**Table 1 Crystal data and structural refinements of 1 at 296 K**

| | | | |
|---|---|---|---|
| Temperature | 296 K | $\gamma$ / (°) | 90 |
| Empirical formula | $C_{23}H_{26}N_8NiS_4$ | $V$ / nm$^3$ | 2.811 2(7) |
| Formula weight | 601.49 | $Z$ | 4 |
| Crystal system | Monoclinic | $\mu$ / mm$^{-1}$ | 1.015 |
| Space group | $P2_1/c$ | $F$(000) | 1 248 |
| $a$ / nm | 0.856 26(13) | Limiting indices | $-11 \leqslant h \leqslant 10, -37 \leqslant k \leqslant 38, -15 \leqslant l \leqslant 15$ |
| $b$ / nm | 2.977 0(4) | $\theta$ range of collection data / (°) | 0.993~27.55 |
| $c$ / nm | 1.180 00(18) | Goodness of fit on $F^2$ | 1.045 |
| $\alpha$ / (°) | 90 | $R_1^a$, $wR_2^b$ (all data) | 0.085 4, 0.108 6 |
| $\beta$ / (°) | 110.839(2) | $R_1^a$, $wR_2^b$ ($I>2\sigma(I)$) | 0.041 4, 0.091 2 |

[a] $R_1=\sum||F_o|-|F_c||/|F_o|$; [b] $wR_2=[\sum w(\sum F_o^2-F_c^2)^2/\sum w(F_o^2)^2]$

**Table 2 Selected bond lengths (nm) and angles (°) for 1**

| | | | | | |
|---|---|---|---|---|---|
| Ni(1)-S(1) | 0.217 88(8) | Ni(1)-S(2) | 0.217 30(9) | Ni(1)-S(3) | 0.217 54(8) |
| Ni(1)-S(4) | 0.217 68(8) | S(1)-C(2) | 0.173 7(3) | S(2)-C(3) | 0.173 7(3) |
| S(3)-C(7) | 0.174 1(3) | S(4)-C(6) | 0.174 0(3) | N(1)-C(1) | 0.114 1(4) |
| N(2)-C(4) | 0.113 7(3) | N(3)-C(5) | 0.114 7(4) | N(4)-C(8) | 0.114 1(4) |
| | | | | | |
| S(2)-Ni(1)-S(3) | 88.30(3) | S(2)-Ni(1)-S(4) | 173.87(4) | S(3)-Ni(1)-S(4) | 92.47(3) |
| S(2)-Ni(1)-S(1) | 92.46(3) | S(3)-Ni(1)-S(1) | 175.43(3) | S(4)-Ni(1)-S(1) | 88.25(3) |
| C(2)-S(1)-Ni(1) | 102.33(10) | C(3)-S(2)-Ni(1) | 102.84(11) | C(7)-S(3)-Ni(1) | 102.67(10) |
| C(6)-S(4)-Ni(1) | 102.68(10) | C(12)-N(5)-C(10) | 107.73(3) | C(12)-N(5)-C(9) | 126.1(3) |
| C(12)-N(6)-C(11) | 107.7(2) | C(12)-N(6)-C(13) | 126.8(3) | | |

## 2 Results and discussion

### 2.1 Crystal structure

Crystal of **1** at 23 ℃ belongs to monoclinic space group $P2_1/c$. As shown in Fig.1a, an asymmetric unit consists of one anion together with one dication. The mean-molecule plane of $[Ni(mnt)_2]^{2-}$ anion, defined by four coordination sulfur atoms, is approximately parallel to the two 1-methyl-imidazolyl rings of the dication with the dihedral angle of 23.3° in the imidazolyl rings containing $N_5$ atom versus 21.7° containing $N_7$ atom. The bond lengths and angles in the planar $[Ni(mnt)_2]^{2-}$ anion, listed in Table 2, are in good agreement with the reported $[Ni(mnt)_2]^{2-}$ compounds[31]. The hydrocarbon chain of the dication adopts the completely *trans*-planar conformation, and two 1-methyl-imidazolyl rings of the dication are arranged in the opposite orientation. The mean molecular planes of two imidazolyl rings of the dication make a dihedral angle of 67.1°.

As displayed in Fig.1b, the $[Ni(mnt)_2]^{2-}$ anions and cations are aligned into segregated columnar stacks along c-axis direction with the very longer Ni⋯Ni and S⋯S distances between the adjacent $[Ni(mnt)_2]^{2-}$

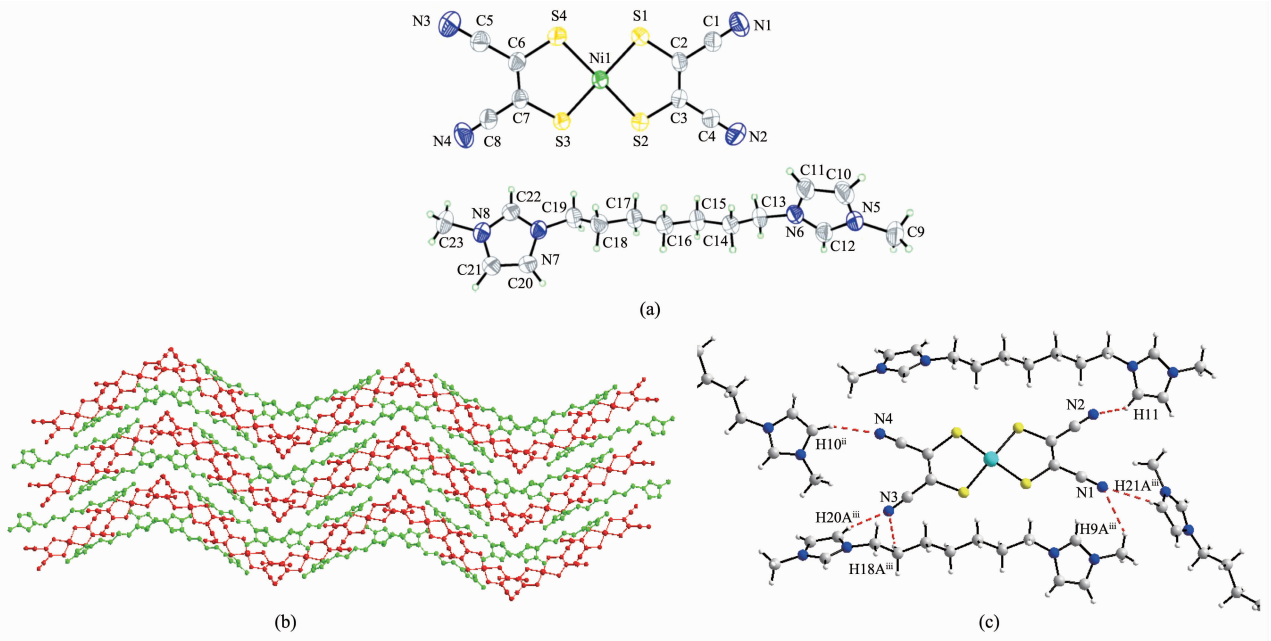


Symmetry code: ⁱⁱ 3−*x*, −0.5+*y*, 1.5−*z*; ⁱⁱⁱ 1+*x*, *y*, −1+*z*; ⁱᵛ 3−*x*, 0.5+*y*, 1.5−*z*

Fig.1　(a) Thermal ellipsoid plots of a single structure at 30% probability level (b) packing diagram viewed along *c*-axis and (c) charge-assisted H···N interactions between the adjacent anion and cation in the crystal of **1**

anions, for instance, $d_{Ni1\cdots Ni1^{i}}$=1.180 0 nm (Symmetry code: ⁱ 1−*x*, −0.5+*y*, *z*). It is noted that the existence of only one type of intermolecular overlap manner in the anion and cation stacks because there are one anion and cation in per repeat unit along stack direction, respectively. Parallel to the *ab*-plane, wave-shape anion chain was formed by neighboring anion column, and anion and cation chains are further aligned into layer structure. In cation layer, two neighboring cations adopt antiparallel arrangement and their 1-methyl-imidazolyl rings are exactly parallel to each other. The relative slippage along the long molecule axis are observed within cation stacks, this kind of overlap pattern minimize the repulsion between the neighboring cation.

It is worth noting that there are charge-assisted H···N interactions between the adjacent anion and cation stacks, as demonstrated in Fig.1c. The shorter interatomic contacts are found with the distances of $d_{N4\cdots H10^{ii}}$=0.240 4 nm, $d_{N3\cdots H20^{iii}}$=0.254 3 nm, $d_{N3\cdots H18A^{iii}}$=0.270 0 nm, $d_{N1\cdots H9A^{iii}}$=0.22.698 nm, $d_{N1\cdots H21^{iv}}$=0.273 3 nm and $d_{N2\cdots H11}$=0.256 nm (Symmetry code: ⁱⁱ 3−*x*, −0.5+*y*, 1.5−*z*; ⁱⁱⁱ 1+*x*, *y*, −1+*z*; ⁱᵛ 3−*x*, 0.5+*y*, 1.5−*z*). Substantial amounts of chain-chain interactions are observed in the cation layer. These charge-assisted H···N interactions and chain-chain interactions are very important in the stabilization of crystal **1**.

### 2.2　Dielectric properties

Frequency dependences of $\varepsilon'$ and $\tan\delta=\varepsilon''/\varepsilon'$ are shown in Fig.2 for **1** in the temperature range of 25~95 ℃. Both dielectric constant and dielectric loss decrease with increase in frequency. The decrease is significant especially at low frequency, which may be electrode polarization and space charge effects. On the other hand, at high frequency, periodic reversal of the electric field occurs so that there is no excess ion diffusion in the direction of electric field. Polarization due to charge accumulation decreases, leading to the observed decrease in dielectric constant and dielectric loss[32]. When the temperature increase, the dispersion region shifts towards higher frequencies due to thermal activation of charge carriers and the $\varepsilon'$ value rise rapidly, indicating the existence of thermally assisted dynamical dipole motion under ac electrical field in **1**, and this is a typical dielectric relaxation behavior. In general, the global polarization of a dielectric material is consisted upon by four different

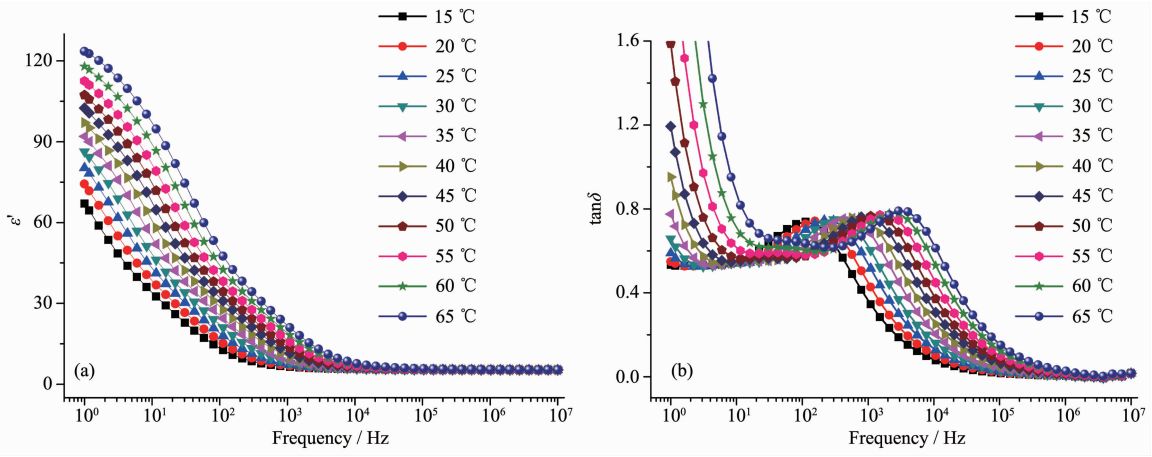


Fig.2 Frequency dependences of (a) $\varepsilon'$ and (b) tan ($\delta$) for **1** in the range of 25~95 ℃

dielectric mechanisms (electronic, atomic, orientation or dipolar, and ionic polarization). At below $10^{12}$ Hz, the dielectric relaxation spectra prevail relating to the behavior of dipole motion or ionic polarization. Therefore, the relaxation that appears in 1 ~$10^5$ Hz could be attributed to dipole or molecular motion in **1**.

The variation of the dielectric loss with the frequency at different temperature is shown in Fig.2b, and a broad peak appears in the tan$\delta$-$f$ plot, indicating that the dielectric relaxation process was observed in the measured frequency windows. It is noted that the peak maximum of dielectric loss shifts towards the high frequency side with the temperature increase from 25 to 95 ℃.

The relaxation process exhibit Arrhenius-type temperature dependence (Fig.3) and is further analyzed according to the empirical Arrhenius relation:

$$\tau=\tau_0\exp(\frac{E_a}{k_B T}) \quad (1)$$

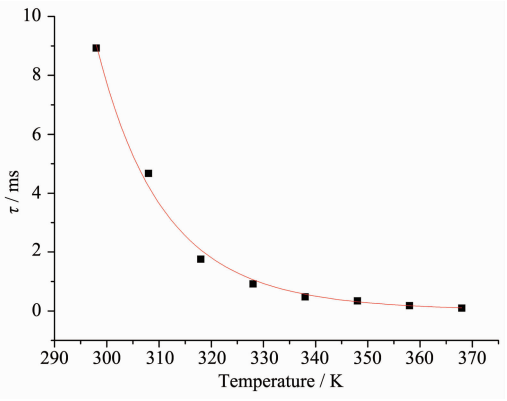


Fig.3 Plots of $\tau$ versus $T$ for **1** at selected temperature

Where $\tau=1/f_{max}$ and $f_{max}$ is the frequency at maximum in the plot of tan$\delta$-$f$ under a selected temperature; $\tau_0$ represents the characteristic macroscopic relation time, $E_a$ is the activation energy or potential barrier, $k_B$ is Boltzmann′s constant. The best fits, using Eq.**1**, gave parameters $\tau_0=6.188(6)\times10^{-13}$ s and $E_a=57.98(3)$ kJ·mol$^{-1}$. The relaxation might be attributed to segmental motion and local molecular oscillation of the alkyl chain.

Fig.4 shows the temperature dependent of the real part of the complex dielectric permittivity $\varepsilon'$ of **1**. As it can be seen, dielectric constant $\varepsilon'$ goes through a broad and pronounced maximum close to 90 ℃ at low measuring frequency. For example, dielectric constant $\varepsilon'$ value is very small ($\varepsilon'\approx8.8$) at 25 ℃ for $f$=1 000 Hz, where thermal motion of the dipole units should be almost suppressed. The $\varepsilon'$ value at 90 ℃ ($\varepsilon'\approx76.1$) for the same frequency measurement was about ten times larger than $\varepsilon'$ value at 25 ℃, which

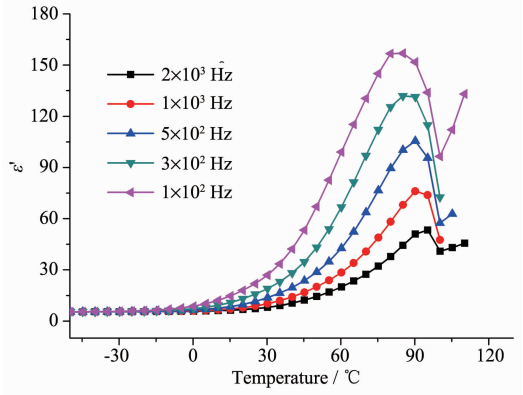


Fig.4 Temperature dependences of $\varepsilon'$ in the selected frequency range of **1**

can be ascribed to the dipole polarization is better able to align in phase with the temperature increase. The large dipole moment, contributed to the dielectric constant $\varepsilon'$ value enhancements in the low-frequency and high-temperature regions, and generated the dielectric peak. The crystal structure at room temperature have the centrosymmetrical space group $P2_1/c$, and no obvious structure phase transition was observed by DSC measurement (see next section). Therefore, a ferroelectric state at high temperature was not expected in the dielectric ground state. As a consequence, the dielectric phase transition probably arises from the disorder-to-order transformation of alkyl chains in the cation moieties. Unfortunately, we failed to obtain the details of the crystal structure in the high temperature phase owing to the bad single crystal X-ray diffraction data above the phase transition.

### 2.3 Thermal properties

The differential scanning calorimetry (DSC) measurements in the range −85 ~230 ℃ for **1** were further carried out for the investigation of the thermal behavior of dielectric phase transition (Fig.5). However, no anomaly is detected near at dielectric phase transition temperature, which indicated such dielectric anomaly shows the second-order phase transition. Only one endothermic event appear in the plots of DSC traces for **1** during the first heating run, and endothermic event occurred around 191 ℃, corresponds to the samples melting. A broad exothermic peak was appeared in the first cooling process, such thermal anomaly may be correspond to the crystallization of **1**, and obvious supercooling behavior with the thermal hysteresis of about 109 ℃ was observed. Such a type of thermal behavior hysteresis often appears in a crystal-to-liquid crystal transformation system and similar $[Ni(mnt)_2]^{2-}$ based compounds, which is thought to be related to the release of structural strain in the heating procedure[24].

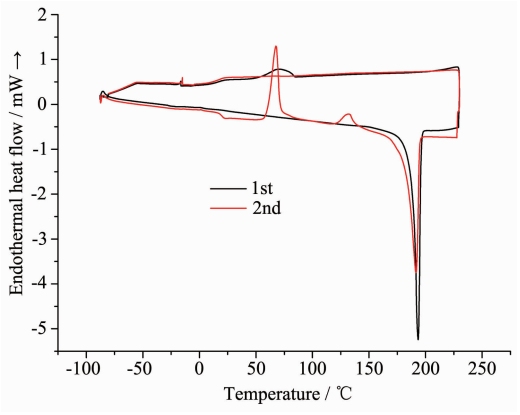


Fig.5 Plots of DSC curves for **1** over the temperature of −85~230 ℃ in the two heating-cooling runs

It is worthy mentioning that **1** exhibits cold crystallization around 66 ℃ and 130 ℃ during the second heating scan, and may be originated from fast cooling rate and the large viscosity. The comparable situation has been seen in polymer systems[33-34], and is very rare in small molecule compounds system.

## 3 Conclusions

In summary, we have present an ion-pair compound **1** comprised of bis (maleonitriodithiolato) nickelate with flexible dication. The packing of bis (maleonitriodithiolato)nickelate anions and dication forms the wave-shape anion chain along *c*-axis direction, respectively. **1** exhibiting remarkable dielectric anomaly, which is probably arise from the disorder-to-order transformation of alkyl chains. The dielectric relaxation process in low-frequency region could be attributed to dipole motion in **1**. Such study provides a possible strategy to explore switchable dielectric material.

**Acknowledgements:** The authors thank National Nature Science Foundation of China for their financial support (grant No. 21201103 and 21301093).

**Supplementary materials:** IR spectra, TG data and PXRD of **1** are included in ESI.

## References:

[1] Simon P, Gogotsi Y. *Nat. Mater.*, **2008**,**7**:845-854
[2] Juarez-Perez E J, Sanchez R S, Badia L, et al. *J. Phys. Chem. Lett.*, **2014**,**5**:2390-2394
[3] Shikata T, Sugimoto N. *J. Phys. Chem. B*, **2012**,**116**:12605-12613
[4] Volksen W, Miller R D, Dubois G. *Chem. Rev.*, **2010**,**110**:56-110

[5] He F K, Yuan C Y, Li K, et al. *RSC Adv.*, **2013**,**3**:23128-23132

[6] Usman M, Lee C H, Hung D S. et al. *J. Mater. Chem. C*, **2014**,**2**:3762-3768

[7] Horiuchi S, Ishii F, Kumai R, et al. *Nat. Mater.*, **2005**,**4**:163-166

[8] Zagorodniy K, Seifert G, Hermann H, et al. *Apply. Phys. Lett.*, **2010**,**97**:251905-251907

[9] Fu D W, Cai H L, Liu Y M, et al. *Science*, **2013**,**339**:425-428

[10]Fu D W, Zhang W, Cai H L, et al. *Adv. Mater.*, **2011**,**23**:5658-5662

[11]Fu D W, Cai H L, Li S H, et al. *Phys. Rev. Lett.*, **2013**,**110**:257061-257061

[12]Fu D W, Zhang W, Cai H L, et al. *Angew. Chem. Int. Ed.*, **2011**,**50**:11947-11951

[13]ZHOU Qin-Qin(周琴琴), Fu Da-Wei(付大伟). *Chinese J. Inorg. Chem.*(无机化学学报), **2013**,**29**(8):1696-1702

[14]Ye Q, Shi P P, Fu X Q, et al. *CrystEngComm*, **2013**,**15**:5307-5313

[15]Sun Z H, Wang X Q, Luo J H, et al. *J. Mater Chem. C*, **2013**,**1**:25621-2567

[16]Li Z Y, Dai J W, Gagnon K J, et al. *Dalton Trans.*, **2013**,**42**:14685-14688

[17]Jain P, Ramachandran V, Clark R J, et al. *J. Am. Chem. Soc.*, **2009**,**131**:13625-13627

[18]Jain P, Dalal N S, Toby B H, et al. *J. Am. Chem. Soc.*, **2008**,**130**:10450-10451

[19]Xu G C, Ma X M, Zhang L, et al. *J. Am. Chem. Soc.*, **2010**,**132**:9588-95590

[20]Akutagawa T, Shitagami K, Nishihara S, et al. *J. Am. Chem. Soc.*, **2005**,**127**:4397-4402

[21]ZHOU Hong(周宏), YU Shan-Shan(于姗姗), DUAN Hai-Bao(段海宝), et al. *Chinese J. Inorg. Chem.*(无机化学学报), **2013**,**29**(7):1-10

[22]Coomber A T, Beljonne D, Friend R H, et al. *Nature*, **1996**, **380**:144-146

[23]XU Duo-Hui(许多慧), SHENG Xiao-Li(盛小利), LU Chang-Sheng(芦昌盛), et al. *Chinese J. Inorg. Chem.*(无机化学学报), **2012**,**28**(5):888-892

[24]Daun H B, Ren X M, Shen L J, et al. *Dalton Trans.*, **2011**, **40**:3622-3630

[25]Daun H B, Yu S S, Liu J L, et al. *Polyhedron*, **2014**,**69**:251-261

[26]Davison A, Holm H R. *Inorg. Synth.*, **1967**,**10**:8-26

[27]Ren X M, Akutagawa T, Nishihara S, et al. *J. Phys. Chem. B*, **2005**,**109**:16610-16615

[28]Tian Z F, Ren X M, Li Y Z, et al. *Inorg. Chem.*, **2007**,**46**:8102-8104

[29]*CrysAlis Ver*1.171, Oxford Diffraction Ltd., Poland, **2004**.

[30]Sheldrick G M. *SHELXL*-97, *Program for the Refinement of Crystal Structure*, University of Göttingen, Germany, **1997**.

[31]Daun H B, Ren X M, Liu J L. *Softs Mater.*, **2014**,**12**:166-178

[32]Ramesh S, Arof A K. *J. Power Sources*, **2001**,**99**:41-47

[33]Zhang J M, Tsuji H, Noda I, et al. *Macromolecules*, **2004**, **37**:6433-6439

[34]Belana J, Pujal M. *Polymer*, **1998**,**10**:1738-1744